

Pamukkale Üniversitesi Mühendislik Bilimleri Dergisi





Mineralogical and geochemical properties of non-marine sedimentary units in Temelli Basin (Polatlı-Ankara)

Temelli havzasındaki (Polatlı-Ankara) karasal sedimanter birimlerin mineralojik ve jeokimyasal özellikleri

Tülay Altay1*

¹Department of Geological Engineering, Faculty of Engineering, Afyon Kocatepe University, Afyonkarahisar, Türkiye. taltay@aku.edu.tr

Received/Geliş Tarihi: 28.02.2025 Accepted/Kabul Tarihi: 21.08.2025 Revision/Düzeltme Tarihi: 20.08.2025 doi: 10.5505/pajes.2025.58492 Research Article/Araştırma Makalesi

Abstract

Study area located in south-west of Ankara in Central Anatolia, is a fault-controlled graben basin. Neogene aged clastic, clayey, dolomitic, tuffitic and evaporitic rocks form dominant lithology in the region. Four deep drillings were made in the field. The basin consists of a quite thick sequence of fluvial and lacustrine units. Fluvial sediments made up of detrital units such as poorly consolidated conglomerate, sandstone, mudstone, siltstone and claystone. Lacustrine sediments commonly made up of fine-grained clastics (mudstone, claystone), carbonates (clayey limestone, marl) and evaporites (sulfates and chlorides). The composition of some levels is almost pure, consisting of one or two evaporite minerals such as halite and anhydrite, while in some levels clay minerals, zeolite and other silicate minerals are present together. Evaporite and non-evaporite units show facies development in vertical and lateral directions. Subhedral lenticular, bar shaped glauberite, cubic halite, rhomboedric dolomite, prismatic celestine, anhydrite and gypsum crystals were observed in SEM studies. Ca, Na, S ions dominate the major element in the evaporate samples. The positive correlation of SiO_2 with K_2O , Al_2O_3 , Fe_2O_3 and TiO_2 indicates the presence of smectite, illite, and feldspar. The high differences (528.8-10061.4ppm) in strontium contents between carbonate and sulfate levels reflect hydrologically unstable conditions and sedimentation in shallow waters. LRE element enrichment relative to HRE elements and Eu anomaly indicated that the basin is upper continental crust origin and fed from a volcanic source.

Keywords: Evaporite, Analcime, Non-marine, Central Anatolia, Neogene Basin

1 Introduction

Temelli Neogene basin is located in the south-western part of Ankara province in Central Anatolia (Figure 1a). Tertiary aged volcanic, sedimentary and volcanosedimentary rocks cover a large area. The basin is a tectonic controlled asymmetric depression area that is associated with other Neogene basins in the area. The region was transformed into inter-mountain basin by the effect of orogenic movements beginning in the Late Cretaceous and remained under the influence of volcanic activity. The NW-SE trending tectonic expansions that lead to the formation of the basin continued from time to time to Pliocene, resulting in volcanic activity in the Quaternary process [1],[2]. The Paleocene-Eocene aged volcanics in Central Anatolia are calc-alkaline arc-volcanics in the subduction zone. The Oligocene, Miocene, Pliocene and Quaternary volcanics are calc-alkaline volcanic rocks which are formed in the subduction zone and are considered to have been originated from

Öz

Çalışma alanı, Orta Anadolu'da Ankara'nın güneybatısında yer alan, fay kontrollü bir graben havzadır. Bölgedeki baskın litolojiyi Neojen yaşlı kırıntılı, killi, dolomitik, tufitik ve evaporitik kayaçlar oluşturur. Sahada dört derin sondaj yapılmıştır. Havza oldukça kalın, akarsu ve gölsel birimler içeren bir istifden oluşur. Akarsu tortuları, zayıf pekişmiş konglomera, kumtaşı, çamurtaşı, silttaşı ve kiltaşı gibi kırıntılı birimlerden oluşur. Gölsel tortular genellikle ince taneli kırıntılılardan (çamurtaşı, kiltaşı), karbonatlardan (killi kireçtaşı, marn) ve evaporitlerden (sülfatlar ve klorürler) oluşur. Bazı seviyelerin bileşimi neredeyse saf olup, halit, anhidrit gibi bir veya iki evaporit mineralinden oluşurken, bazı seviyelerde kil mineralleri, zeolit ve diğer silikat mineralleri bir arada bulunur. Evaporit ve evaporit olmayan birimler yanal ve düşey yönde fasiyes gelişimi gösterir. SEM çalışmalarında subhedral merceksi, çubuk şekilli globerit, kübik halit, romboedrik dolomit, prizmatik sölestin, anhidrit ve jips kristalleri gözlenmiştir. Ca, Na, S iyonları evaporit örneklerinde majör element olarak baskındır. SiO₂ ile K₂O, Al₂O₃, Fe₂O₃ ve TiO₂'nin pozitif korelasyonu simektit, illit ve feldispatın varlığını gösterir. Karbonat ve sülfat seviyeleri arasındaki stronsiyum içeriklerindeki yüksek farklar (528.8-10061.4ppm) hidrolojik olarak duraysız koşullar ve sığ sularda çökelmeyi yansıtmaktadır. ANT elementlerine göre HNT element zenginleşmesi ile Eu anomalisi havzanın üst kıtasal kabuk kökenli olduğunu ve volkanik bir kaynaktan beslendiğini göstermektedir.

Anahtar kelimeler: Evaporit, Analsim, Karasal, Orta Anadolu, Neojen Havza

continental crust [3]. The basin is located in the southwest part of the Beypazarı basin. In the study area, Hançili formation containing evaporitic sequence is correlated with the Hırka Formation located in Beypazarı basin. There are two different levels of trona in the Hırka Formation, as well as bituminous shale and lignite deposits. Beypazarı trona bed is one of the few known in the world.

In the region, coal exploration drillings were carried out by Turkish Coal Enterprises (TKI). These drillings were examined within the scope of the project. Previous studies in the region have been directed to the geological, geochemical, sedimentological, paleontological and tectonic evolution of the Neogene basins [4]-[18]. Despite the availability of substantial data from previous studies, the study area remains ambiguous, primarily due to the embedded the lacustrine sediments. This study aims to identify the lateral and vertical distributions of the sedimentary units in deep drilling, and to research their mineralogical and geochemical properties.

1

^{*}Corresponding author/Yazışılan Yazar

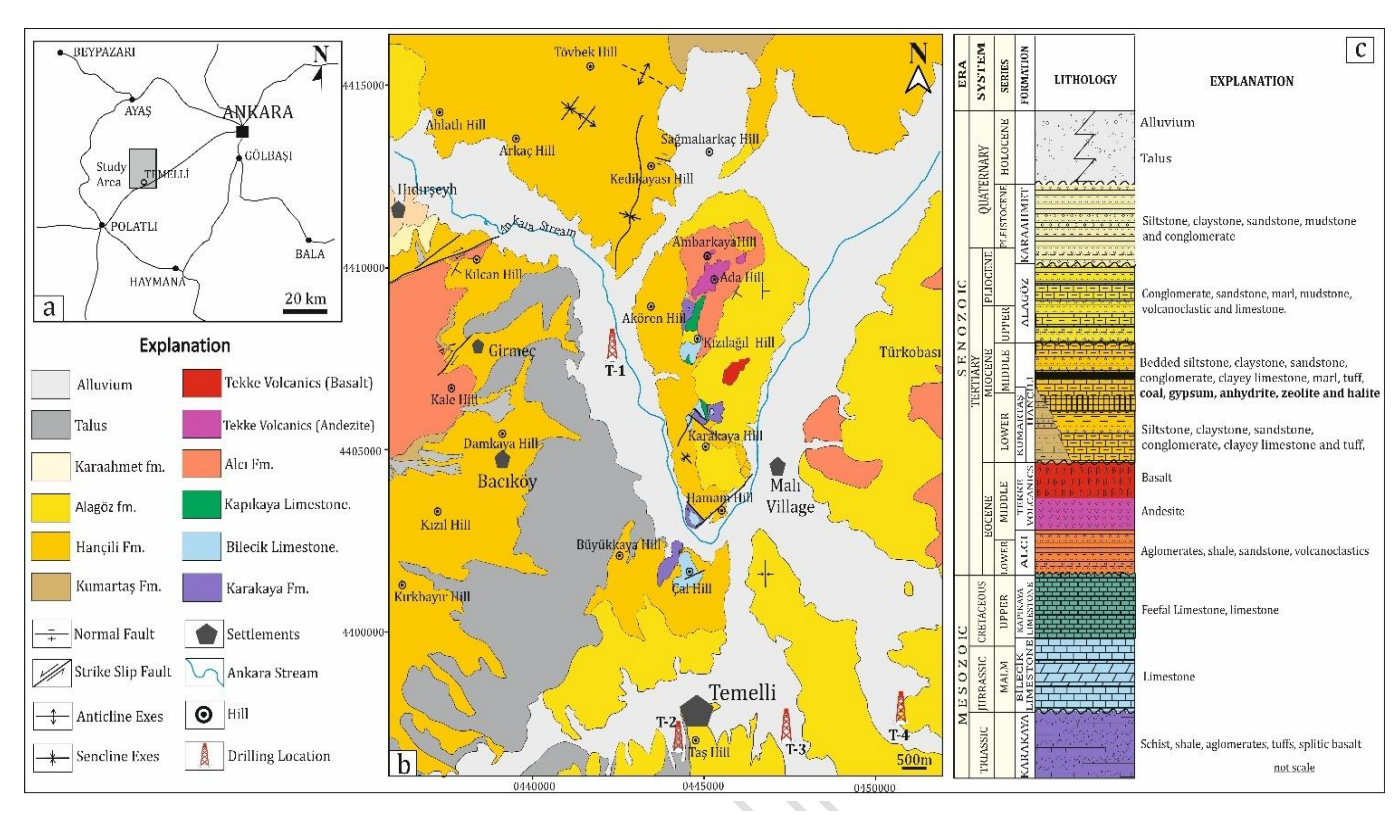


Figure 1 a) Location map of the study area, b) geological map of the study area and the locations of drilling points in the basin (geological map modified from [5],[11]), c) generalized stratigraphic section of the study area (modified from [11]).

2 Geological setting

In study area and surrounding, geological units formed from Triassic to Quaternary (Figure 1b and c). Most of the basement rocks compose Triassic metamorphic rocks belonging to the Karakaya formation in the study area. The Triassic aged Karakaya Formation predominantly consists of green-red argillaceous schist, mica schist and locally quartz schist, in the part low-grade metamorphosed sandstones, conglomerates, sandy limestones, mudstones, shales, tuffs, agglomerates, spilitic basalts and accompanying Permian aged limestone blocks [5],[11]. The Upper Jurassic-Lower Cretaceous aged Bilecik limestones, which are composed of shelf-type carbonates, unconformably cover the Karakaya Formation. Bilecik aged limestones conformably overlain by The Maastrichtian (Late Cretaceous) Kapıkaya limestones, composed of reefal limestone [5],[11]. These three formations are outcropping in narrow areas in the examination area. After deposition of Kapıkaya limestones, the region risen and transits to the terrestrial position. Afterwards, the basin collapsed again, and the detritals of the Lower-Middle Eocene aged Alcı Formation, which was exposed in the northwestern part of Bacıköyü and around Ada Tepe, precipitated. At this time, along with sedimentation, basaltic and andesitic volcanism continued (Middle Eocene) [5],[11]. Tekke volcanics are divided into two members, namely Andesite and Basalt in the region (Figure 2a and b). These volcanic rocks are exposed in the vicinity of Ankara Stream, Ada Hill and Kızılağıl Hill in the study area. The Lower-Middle Miocene aged Kumartas Formation, which are exposed at small areas in the north-east of the study area, unconformably overlies Tekke volcanics. Kumartaş Formation made up of conglomerate, sandstone, siltstone, claystone, tuff and clayey limestone. It is usually red, light green and gray [5],[11]. The Lower-Middle Miocene aged Hançili Formation, widely observed throughout the study area, conformably overlies the Kumartaş Formation. The unit consists of intercalations of fine-to-middle bedded siltstone, claystone, sandstone, conglomerate, clayey limestone, marl, tuff, gypsum, anhydrite and halite (Fig 2c and d). All of these sediments accumulated within fluvial and shallow lacustrine environments. Furthermore, the unit contains coal levels [5],[11]. The volcanic activity continues during sedimentation. Hançili Formation can be correlated with the lacustrine limestones [19], Middle-Late Miocene sediments [20], Kavaklı Formation [21],[22], Hirka formation [23] and the upper parts of Aktepe formation [24] which spread in Central Anatolia Region. Hançılı Formation unconformably overlain by the Upper Miocene-Pliocene aged Alagöz Formation consisting of conglomerate, sandstone, marl, mudstone, and limestone (Figure 2e and f). The unit comprises fan-stream and minor lacustrine additives at its base, followed by lacustrine limestones, and contains volcano-pyroclastics in the upper levels. Alagöz Formation overlain by the Late Pliocene-Early Pleistocene aged Karaahmet Formation consists of siltstone, claystone, sandstone, mudstone and conglomerate [5],[11]. In the southwest of the study area commonly precipitated Quaternary aged talus and alluvium observed along the Ankara stream is the youngest units in the region.

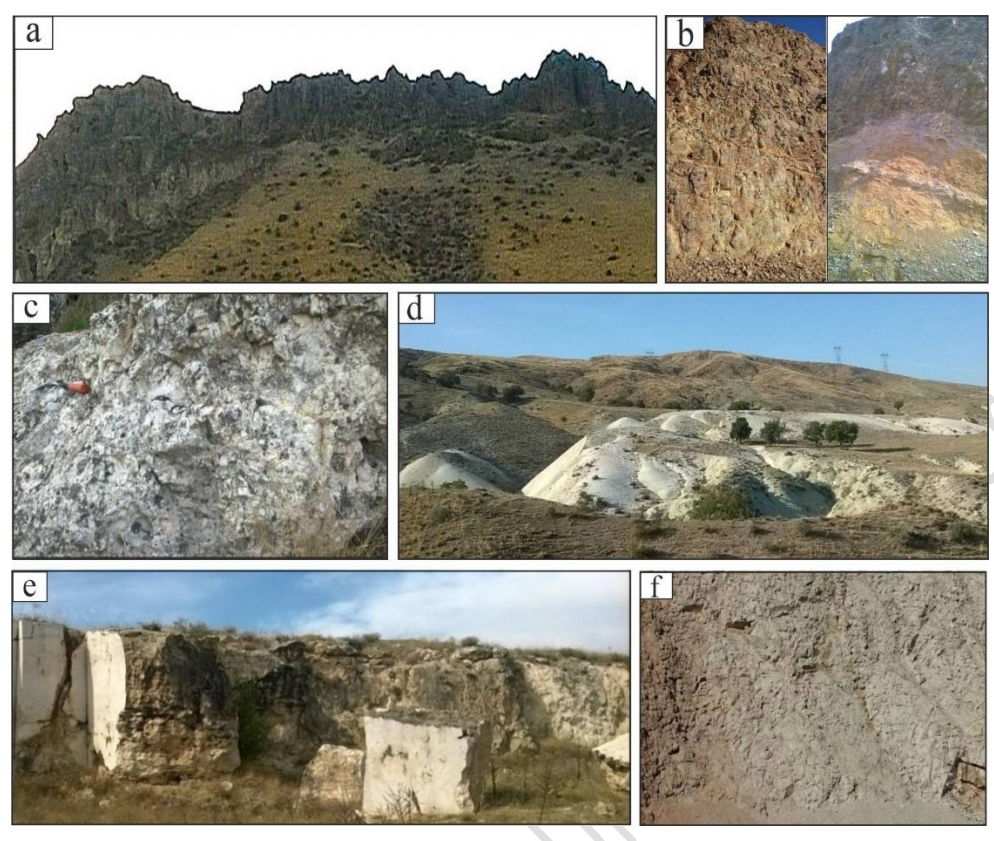


Figure 2 Outcrop photos from study area a) andesites of Tekke volcanics (around the Ada hill), b) basalts of Tekke volcanics (north of the organized industrial zone) c) closing view of limestone in the Hançili Formation (west of the Ankara stream), d) Marn in the Hançili Formation (north of the Girmeç village), e) limestone in the Alagöz Formation (west of the Ankara stream), f) fluvial units of the Alagöz Formation.

3 Material and methods

The investigations conducted in the area included both field studies and laboratory analyses. During the fieldwork, representative samples were collected from the four drillings ((T1 (641 m long), T2 (365 m), T3 (379 m) and T4 (215.5 m)) drilled by TKİ for coal exploration (Fig. 1b). Meters of samples taken from the drillings were designated; T1, T2, T3 and T4 symbols represent different drillings from the tables. Drillings have been correlated with each other, and 53 compiled samples were performed in mineralogical analyses. The mineralogical composition of the whole-rock and clay-size fractions (< 2 μm) were determined by X-ray diffraction (XRD) in the Afyon Kocatepe University laboratories using a Shimadzu 6000 and Bruker D8 Advance X-ray powder diffractometer with a graphite monochromator and Ni-filtered CuKa radiation; powders were scanned from 2° to 70°/min. Clay minerals were determined using three XRD patterns (air-dried at 25°C, ethylene-glycolated, and heated at 490°C for 4 h) of the claysized fractions (< 2 μm). Mineral identification was performed according to [25]. Mineral morphologies and interrelationships were investigated using scanning electron microscopy (SEM) and electron diffraction spectrometry (EDS) in in the Afyon Kocatepe University laboratories. The SEM studies were performed using a Leo 1430VP model SEM, equipped with EDS using an accelerated voltage of 20 kV. Spot chemical analyses of sulfate and carbonate minerals were performed using energydispersive spectrometry (EDS). A beam current of 15 nA, a

beam diameter of 5 μm , and a ZAF correction scheme were used in the study.

In addition, for chemical analysis, 32 clay, carbonate and evaporite rich samples have been systematically compiled from the Temelli drilling logs (T-1, T-2 and T-3). Chemical analyses of samples (major-oxide contents) were performed using ICP-ES, trace- and rare-earth elements (REE) from ICP-MS and total carbon (TOT/C) and sulfur (TOT/S) from Leco at Acme Analytical Laboratories Ltd. (Canada). Loss on ignition (LOI) was calculated from the weight loss after heating 2 g of sample at $1000~^{\circ}\text{C}$ for 2 h. The detection limits of the elements were 0.01-0.1 ppm for REE and 0.1-20 ppm for trace elements.

4 Results

4.1 General properties of the investigated drillings

The depth of the T1 drilling in the central part of the basin is 641m (Figure 1 and Figure 3). A very thick evaporitic sequence was identified in the T1 drilling. The basement rocks are Eocene turbidites and crystallized limestone in the drilling. The units that characterize the fluvial and lacustrine environment of Hançili Formation were observed in the drilling section. The Temelli-1 drilling consists of unconsolidated sand and clay in the upper levels characterizes the fluvial environment (surface down to $20\ m$).

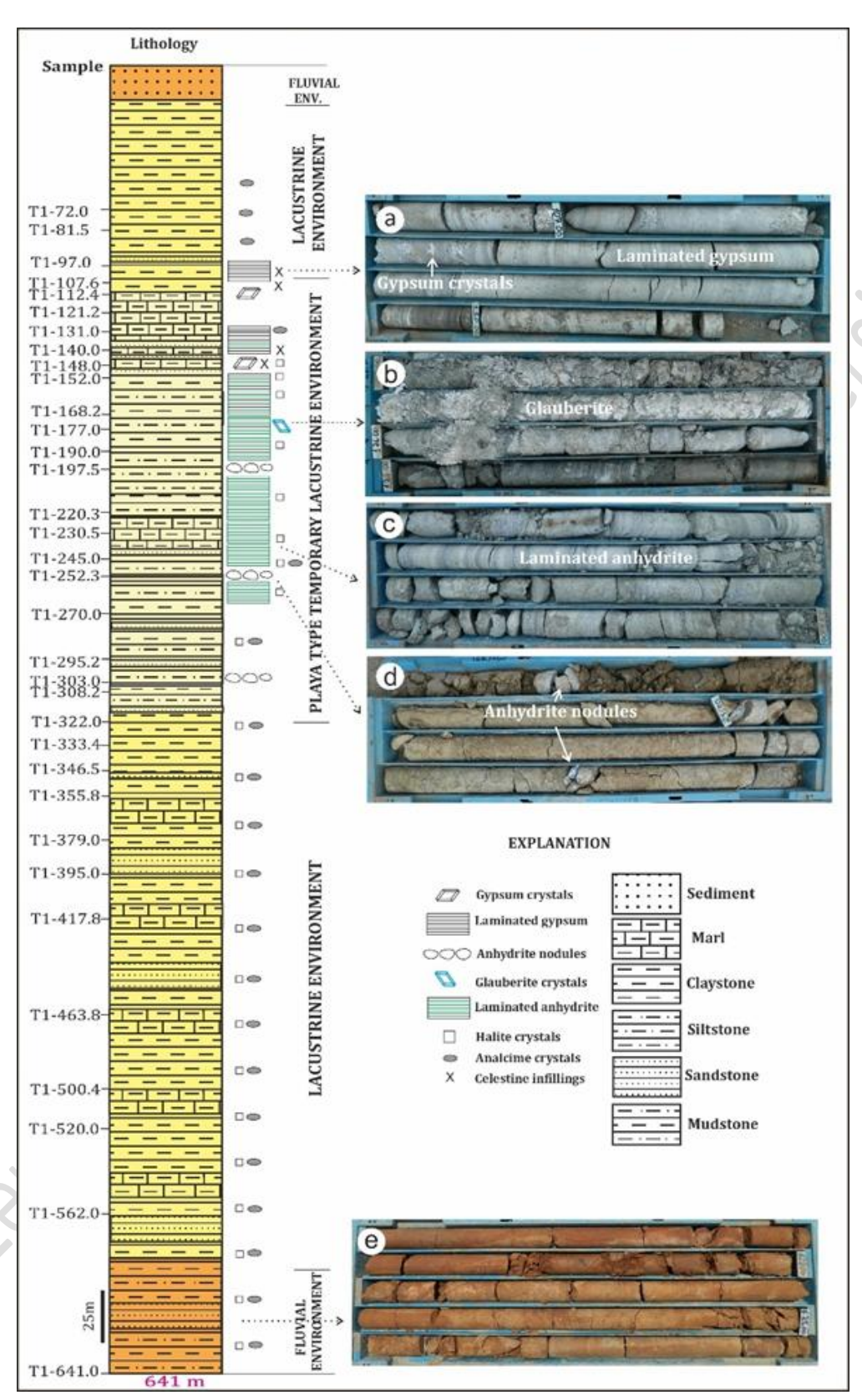


Figure 3 Vertical distribution of the lithology in the Temelli-1 drilling (Core photographs a to e). Photos: a) green claystone containing gypsum crystals and alternation of clay, gypsum and carbonate laminations, b) salt zone containing gypsum, anhydrite, glauberite, c) alternation of clay, anhydrite and carbonate laminations, d) calcareous green claystone containing anhydrite nodules, e) brown calcareous mudstone.

The Temelli-1 drilling consists of a weakly consolidated, lightdark greenish, terrestrial pebbly carbonated claystone layer was observed between 20 and 90m. Between 90 and 105m, weakly consolidated, light gray-greenish, fine-grained sandstone, pebbly sandstone and claystone with occasional laminated marl alternation were observed. The Temelli-1 drilling consists of a weakly consolidated, laminated, light graygreenish marl and claystone, gypsum and little anhydrite between 105 and 148 m (Figure 3a). Laminated claystone and fine-grained sandstone strata are among the gypsiferous layers. Temelli-1 drilling consists of a weakly consolidated light gray claystone between 148 and 160 m. There is calcareous laminated claystone, anhydrite between 160 and 175 m. After this layer, there is a salt zone with 2-4 m thick in whitishgrayish color, containing glauberite, halite, anhydrite and gypsum minerals (Figure 3b). Temelli-1 drilling consists of weakly consolidated, light gray, cross-bedded, carbonated clayey-siltstone, claystone with anhydrite nodules, laminated marl, claystone, halite, anhydrite layer alternation between 180 and 245 m (Figure 3c). Temelli-1 drilling consists of weakly consolidated, green terrestrial sandstone intercalated with claystone-mudstone containing anhydrite nodules between 245 and 304 m (Figure 3d). Light gray mudstone, conglomerate, and intercalated fine-grained sandstone layers were observed between 304 and 318m. Weakly consolidated, light grayish-

greenish sandstone intercalated with claystone-marl layers containing halite and analcime shows continuity from 318 m to 580 m. It has reddish-brownish colored mudstone occasional intercalated sandstone in places that characterizes the fluvial environment from 580 to 641 m (Figure 3e).

The units that characterize the fluvial and lacustrine environments of the Alagöz Formation have been defined in the drilling of Temelli 2. The Temelli 2 drilling consists of unconsolidated sand and clay in the upper levels (surface down to 30 m). Lacustrine deposits consisting mainly of weakly consolidated calcareous mudstone, laminated claystone and marl alternations were identified between 30 and 100 m of the drilling (Figure 4a). There are gastropods in the marl and mudstones. It has a brown and gray colored, medium to weakly consolidated mudstone, claystone, marl and sandstone alternation between 100 and 320 m in the drilling (Fluviolacustrine sequence) (Figure 4b). The Temelli 2 drilling consists of greenish gray colored, weakly consolidated, poorly sorted, conglomerate terrestrial laminated sandstone and intercalations (Fluvial sequence) between 320 and 350 m. Yellowish-brown to grayish, consolidated, poorly sorted widespread quartz pebble conglomerate and terrestrial sandstone intercalations (Eocene aged turbiditic basement rocks) were observed between 350 and 365 m of the drilling.

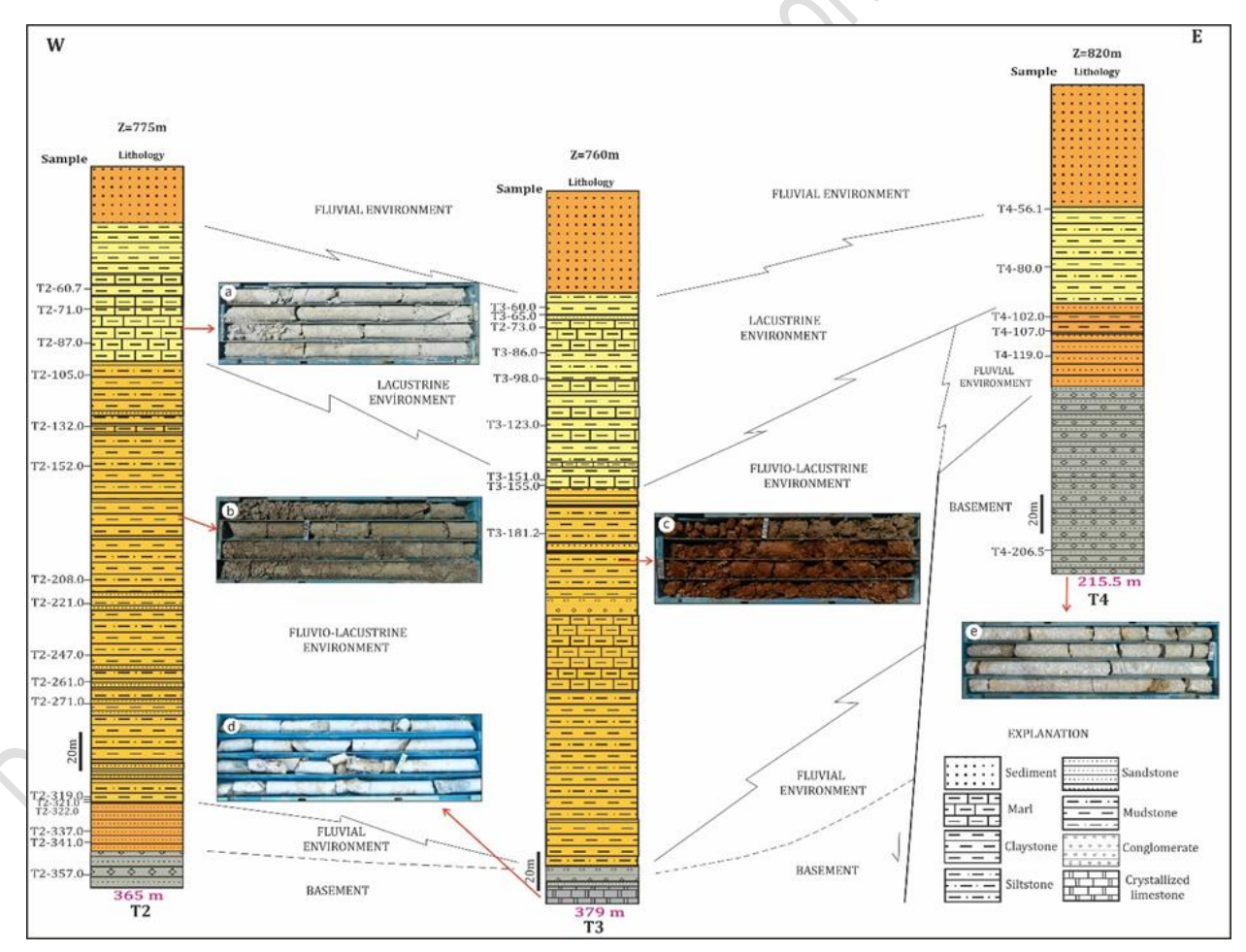


Figure 4 Lithological correlation of drilling logs (T2, T3 and T4) and depositional systems from W-E in the south of Temelli basin (Core photographs a to e). Fotos; a) gray clayey carbonate (T2), b) green weakly consolidated claystone (T2), c) weakly consolidated calcareous mudstone (T3), d) crystallized limestone (Eocene-Basement) (T3), e) well-consolidated turbiditic conglomerates of the basement (T4).

The units that characterize the fluvial and lacustrine environments of the Alagöz Formation have been defined in the drilling of Temelli 3. The Temelli 3 drilling consists of unconsolidated sand and clay in the upper levels (surface down to 55 m). Lacustrine sequence consisting mainly of calcareous mudstone, claystone and marl alternations was identified between 55 and 157 m of the drilling. There are gastropods in the marl and mudstones. The Temelli 3 drilling consists of yellowish-brown and light gray colored, medium to weakly consolidated mudstone, calcareous mudstone and sandstone alternation between 157 and 350 m (Fluvio-lacustrine sequence) (Figure 4c). Yellowish-grayish, consolidated, poorly sorted, terrestrial laminated sandstone and conglomerate intercalations (fluvial sequence) were observed between 350 and 370 m of the drilling. Medium to dark grayish, common calcite veined crystallized limestone (Eocene-Basement) were identified between 370 and 379 m of the drilling (Figure 4d).

The units that characterize the fluvial and lacustrine environments of the Alagöz Formation have been defined in the drilling of Temelli 4. The Temelli 4 drilling consists of unconsolidated sand and clay in the upper levels (Fluvial sequence) (surface down to 50 m). Lacustrine sequence consisting of thin-layered, calcareous mudstone with gastropods and laminated claystone was identified between 50 and 96 m of the drilling. The Temelli 4 drilling consists of yellowish gray colored, medium-consolidated, poorly sorted sandstone, conglomerate, and weakly consolidated claystone between 96 and 135 m (Fluvial sequence). Medium to dark grayish, consolidated sandstone and conglomerate alternations (Eocene-Basement) were observed between 135 and 215.5 m of the drilling (Figure 4 e). Correlations of the drillings in the basin indicate that the Neogene sequence filling this basin is composed of transgressive and regressive sedimentary series from top to bottom (Figure 4).

4.2 Mineralogical properties

Evaporite minerals in the basin consist of carbonates (calcite and dolomite), sulphates (gypsum, anhydrite, glauberite and celestine) and chlorides (halite). Clay minerals, zeolite (analcime), quartz and feldspar were also identified in the study area. Quartz, feldspar and clay minerals are in the clastic fraction of the sediments and they are especially present in the middle and marginal part of the basin. Calcite and dolomite are the main carbonate minerals in the basin. Calcite is present in the all drillings. While dolomite is not found in the T 4 drilling, it is commonly found in other drillings [13]. Sulfate minerals are only present in the T1 drilling section from the central part of basin. Gypsum and anhydrite were dominant sulfate minerals in the basin. Glauberite is only found between 175m and 178m in T1 drilling. Celestine is also present in the upper level of the T1 drilling sections (Figure 3). Gypsum was the major sulfate mineral in the upper profile, whereas anhydrite was common sulfate minerals in the lower levels of the drilling. Halite is the evaporite mineral in the center of the basin and present in the middle and lower profile of the drilling well (T1 drilling). Analcime is the zeolite mineral in the center of the basin, and present in the upper and lower profile of the Temelli-1 drilling section (Figure 3). The main clay mineral assemblage consists of Ca-Na-smectite, illite, chlorite and kaolinite [10].

In the SEM studies, it is observed that the gypsum crystals with unidirectional cleavage have euhedral and subhedral (Figure 5a). Prismatic anhydrite crystals with two-directional crystal growth traces were observed in microcrystalline matrix.

In the EDX analysis, anhydrite crystals were found to contain high S and Ca (Figure 5c). It is observed that celestine crystals are euhedral and subeuhedral prismatic. EDX semi-quantitative analysis showed celestines have high Sr and S (Figure 5d and e). Illite mineral, which has a plate-like structure, has been observed together with rhomboedric dolomite crystals (Figure 5f). It is observed that euhedral prismatic felspar crystal (Figure 5g). Halite crystals are subhedral (cubic) (Figure 5h). In the EDX analysis, halite crystals were found to contain high Cl, Na and low Ca (Figure 5i). It is observed that glauberite crystals are subhedral and unhedral, lenticular and bar shaped in the Temelli basin (Figure 5j and l). In the SEM studies, it is observed that glauberite is surrounded by anhedral cubic halite crystals. In some SEM images, dissolution traces were detected on the surface of halite (Figure 5j). EDX semi-quantitative analysis showed glauberites have high S and low Ca, Na (Figure 5k).

4.3 Chemical composition of lacustrine sediments

The distribution of the major element oxide, LOI, total C (TOT/C) and total S (TOT/S) contents (%) of the samples were given in Table 1. Since C and S contents could not be measured with ICP-MS analysis, Sum values were low in the samples containing carbonate and sulfate. C and S contents of the samples were measured with Leco analysis and added to the table. Based on the carbon (C) and sulfur (S) contents of the samples, CO_2 and SO_3 contents were calculated and presented in Table 1. High SiO2, Al2O3, Fe2O3, K2O and TiO2 levels were observed in the abundance of quartz, felspar and other clastic and terrigenous minerals. In addition, the high Al₂O₃ content indicates that the amount of clay minerals, especially illite, is contained at a higher rate than other samples when evaluated together with K₂O [26]. SiO₂ and Al₂O₃ contents of T2 and T3 drilling samples ranged from 23.12 to 57.57% and 6.20 to 16.23%, respectively. SiO2 and Al2O3 contents of T1 drilling samples ranged from 0.78 to 49.28% and 0.14 to 14.53%. respectively. The positive correlation of SiO₂ with K₂O₃, Al₂O₃, Fe₂O₃ and TiO₂ indicates the presence of smectite, illite, and feldspar (Figure 6a-d). Calcite and dolomite were present throughout the drilling profiles in variable amounts. In the carbonate-rich samples (T1-116.5, T1-194.5, T1-241, T2-87.0, T2-132.5, T3-73.0, T3-98.2 and T3-151) the MgO, CaO and LOI contents were high. Their MgO contents were between 4.86% and 14.86%, and their CaO contents were between 10.58% and 25.64%. Their LOI and CO₂ contents ranged from 21.7 to 37.1% and from 15.40 to 30.58%, respectively.

CaO and Total S were high in the samples containing Ca-Na sulfates (gypsum, anhydrite and glauberite). Sulfate-rich samples (T1-101.6, T1-107.6, T1-131, T1-161, T1-177, T1-252.3 and T1-303) were enriched with CaO content (21.56-40.97%) and SO_3 content (25.58-57.53%) whereas the contents of other oxides were decreased in these samples (Figure 6e).

Covariance between the Ca and total S was found in the sulfaterich samples. Elevated Ca and total S concentrations were observed at the upper and middle parts of the T1 drilling. Covariance between Ca and total C was observed due to the presence of calcite and dolomite in carbonate-rich samples. Concentrations of Na⁺ ions were the highest (10.77%) in the glauberite sample (T1-177). In the halite and analcime-rich samples, Na contents were between 1.80% and 4.42%. Concentrations of Na⁺ ions were distinctly higher in the middle and lower parts of the T1 drilling.

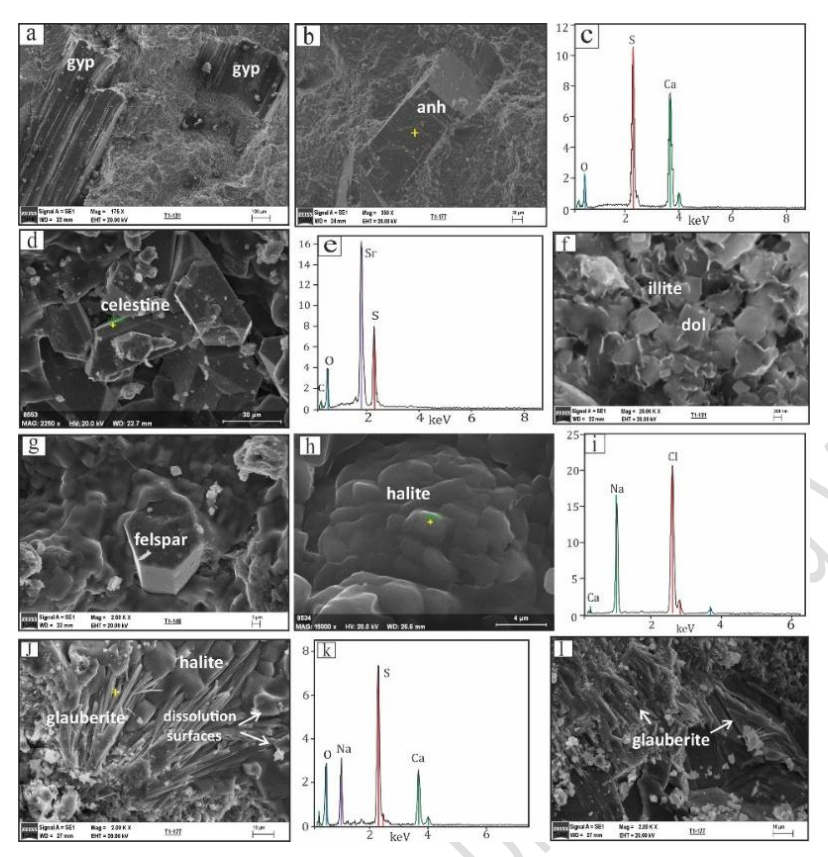


Figure 5 a) SEM images of euhedral gypsum (gyp) crystals with unidirectional cleavage (T1-131), b) SEM images of prismatic anhydrite (anh) crystals with two-directional crystal growth traces (T1-177), c) EDX analysis of anhydrite, d) SEM images of prismatic and lenticular celestine crystals (T1-148), e) EDX analysis of celestine, f) SEM images illite plates in the rhomboedric dolomite (dol) crystals (T1-131), g) SEM images euhedral prismatic felspar crystal (T1-148), h) SEM pictures of subhedral halite crystals (T1-152), i) EDX analysis of halite, j) bar shaped glauberites and anhedral halite crystals, dissolution surfaces of halite, k) EDX analysis of glauberite, l) SEM images of subhedral lenticular and bar shaped glauberite (T1-177)

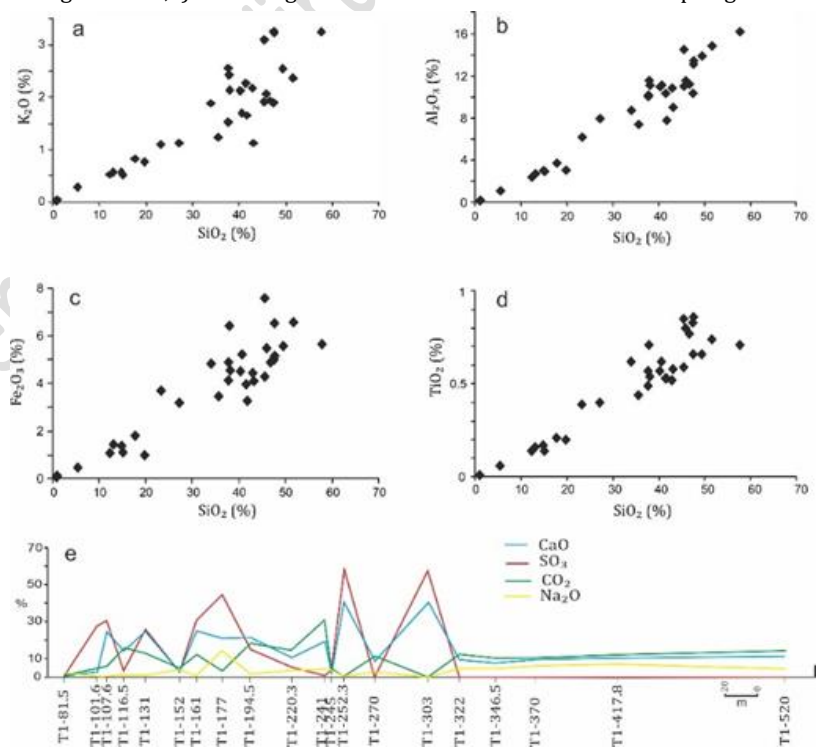


Figure 6. Elemental variation diagrams for major oxides of Temelli basin samples a) K₂O vs. SiO₂, b) Al₂O₃ vs. SiO₂, c) Fe₂O₃ vs. SiO₂, d) TiO₂ vs. SiO₂, and e) vertical distribution of CaO, Na₂O, CO₂ and SO₃ of T1 drilling.

Та	Table 1. Major element oxide, LOI, total C, total S, CO ₂ and SO ₃ contents (%) of the samples selected from drillings														s		
Sample	SiO ₂	Al_2O_3	Fe_2O_3	MgO	Ca0	Na_2O	K_2O	TiO ₂	$P_{2}O_{5}$	MnO	Cr_2O_3	LOI	Sum	Total C	Total S	CO_2	SO ₃
T1-81.5	49.28	13.91	5.57	10.76	0.94	2.41	2.55	0.66	0.21	0.06	0.02	13.5	99.88	0.33	0.29	1.21	0.73
T1-101.6	14.68	3.03	1.38	3.78	25.55	0.66	0.57	0.17	0.06	0.03	0.011	21.5	71.42	1.63	11.57	5.98	28.93
T1-107.6	14.95	2.96	1.11	4.46	24.47	0.76	0.52	0.14	0.04	0.02	0.008	20.8	70.3	1.7	11.83	6.23	29.58
T1-116.5	35.45	7.42	3.46	12.91	13.75	1.84	1.24	0.44	0.12	0.09	0.027	21.7	98.55	4.45	1.14	16.32	2.85
T1-131	12.93	2.74	1.44	8.9	25.12	1.04	0.57	0.16	0.04	0.04	0.009	23.3	76.3	3.58	10.23	13.13	25.58
T1-152	42.75	10.87	4.44	13.58	2.3	3.95	2.18	0.52	0.17	0.07	0.014	19	99.9	1.42	1.18	5.21	2.95
T1-161	12.17	2.42	1.08	12.07	24.37	1.1	0.53	0.14	0.02	0.02	0.009	16.1	70.1	3.23	12.42	11.84	31.05
T1-177	5.29	1.12	0.47	3.23	21.56	14.51	0.29	0.06	0.01	0.01	0.003	7.4	53.94	0.87	17.93	3.19	44.83
T1-194.5	17.58	3.75	1.81	12.05	21.15	2.42	0.83	0.21	0.05	0.04	0.01	25	84.95	4.95	5.93	18.15	14.83
T1-220.3	33.84	8.76	4.83	12.7	10.81	3.42	1.89	0.62	0.14	0.09	0.029	22.7	99.87	3.94	2.01	14.45	5.03
T1-241	19.62	3.08	0.99	14.86	19.02	3.89	0.77	0.2	0.03	0.03	0.016	37.1	99.57	8.34	0.19	30.58	0.48
T1-245	45.31	14.53	7.58	6.71	3.07	3.77	3.1	0.85	0.11	0.06	0.036	14.7	99.85	1.26	1.54	4.62	3.85
T1-252.3	0.78	0.14	0.07	0.08	40.6	0.08	0.02	0.01	0.01	0.01	0.002	1.1	42.91	0.06	23.01	0.22	57.53
T1-270	37.75	11.59	6.42	9.43	8.4	2.88	2.43	0.71	0.14	0.11	0.029	19.9	99.86	3.06	0.18	11.22	0.45
T1-303	0.86	0.22	0.13	0.11	40.97	0.13	0.05	0.01	0.01	0.01	0.002	1.9	44.41	0.05	22.93	0.18	57.33
T1-322	40.12	11.01	4.51	7.08	9.12	5.03	2.13	0.57	0.12	0.09	0.017	20	99.83	3.36	0.37	12.32	0.93
T1-346.5	45.32	11.05	4.29	6.35	8.51	4.76	1.92	0.59	0.11	0.08	0.021	16.8	99.85	2.84	0.31	10.41	0.78
T1-370	41.34	10.37	3.97	5.47	9.6	5.75	2.27	0.53	0.08	0.08	0.016	20.3	99.78	2.99	0.18	10.96	0.45
T1-417.8	37.92	11.13	4.55	6.35	10.76	5.96	2.14	0.54	0.08	0.09	0.015	20.2	99.8	3.27	0.18	11.99	0.45
T1-520	37.54	10.08	4.13	7.52	11.48	4.4	2.56	0.49	0.06	0.08	0.016	21.4	99.85	3.9	0.12	14.30	0.30
T2-60.7	47.4	13.14	6.53	2.89	8.48	0.93	3.26	0.66	0.04	0.07	0.023	16.4	99.86	2.06	0.04	7.55	0.10
T2-87	23.12	6.2	3.7	6.95	25.64	0.75	1.1	0.39	0.08	0.25	0.015	31.6	99.82	7.96	0.02	29.19	0.05
T2-105.4	47.31	10.38	5.0	3.63	10.92	1.32	1.9	0.83	0.15	0.07	0.036	18.2	99.78	3.06	0.03	11.22	0.08
T2-132.5	41.58	7.8	3.27	5.53	15.57	1.12	1.66	0.53	0.08	0.16	0.031	22.4	99.81	5.12	0.03	18.77	0.08
T2-152.5	45.73	11.57	5.48	3.15	10.72	1.29	2.07	8.0	0.16	0.08	0.029	18.6	99.8	2.7	0.05	9.90	0.13
T2-208	46.54	11.25	4.89	3.01	11.07	1.25	1.94	0.77	0.17	0.09	0.031	18.8	99.81	3.04	0.03	11.15	0.08
T2-319.3	57.57	16.23	5.65	2.55	0.59	1.43	3.25	0.71	0.09	0.03		11.7	99.86	0.08	1.47	0.29	3.68
T2-337.3	47.46	13.48	5.16	1.39	12.97	1.09	3.23	0.86	0.11	0.06	0.022	14	99.88	3.12	0.28	11.44	0.70
T3-60.4	40.46	11.15	5.22	3.93	14.0	1.15	1.7	0.62	0.08	0.07	0.031	21.4	99.8	3.57	0.05	13.09	0.13
T3-73	27.03	7.98	3.19	6.63	22.26	0.97	1.13	0.4	0.05	0.06	0.017	30	99.78	6.74	0.09	24.71	0.23
T3-86	51.47	14.87	6.57	3.46	2.81	1.43	2.37	0.74	0.08	0.05	0.027	15.9	99.82	0.91	0.06	3.34	0.15
T3-98.2	37.57	10.22	4.89	8.55	10.58	1.3	1.53	0.57	0.05	0.09	0.025	24.3	99.73	4.61	0.09	16.90	0.23

Trace element contents (ppm) of the samples were given in Table 2. Sr content in the samples varies between 127.4 ppm and 10061.4 ppm. Evaporite-rich samples had higher Sr contents, compared with the detrital-rich sediments; clay-rich samples had relatively low Sr contents (127.4-720.8 ppm). In the carbonate-rich samples, the Sr contents ranged from 958.3 to 1391.0 ppm. In addition, gypsum-rich samples were low in Sr levels (528.8 ppm). In the purest anhydrite samples (T1-252.3 and T1-303), Sr contents were 1304.8 ppm and 1321.1 ppm, respectively. Glauberite-rich sample (T1-177) was high Sr contents (1376.5 ppm). In the halite and analcime-rich samples the Sr contents ranged from 504.2 to 959.8 ppm. In the samples containing celestine (T1-107.6 and T1-116.5), Sr contents were 7201.9 ppm and 10061.4 ppm, respectively.

4.1

4.86

13.14

1.4

1.13 0.58

0.05

0.07

0.036

22.4 99.86

T3-151

42.98

9.04

In the analyzed samples, Ba; varies between 8-936 ppm, Rb; 0.8-141.9 ppm, Zr; 2.8-194.1 ppm, Sc; 1-22 ppm, V; 18-196 ppm, Y; 0,4-21,2 ppm. Total REE contents of the samples ranged from 2.01 to 168.65 ppm. The REE (Rare Earth Elements) and some other trace elements (V, Sc, Cr, Co, As, Ba, Rb, Th) contents are higher in the clay-rich samples than in the evaporite-rich samples (sulfates and chloride); the carbonate-rich samples had an intermediate REE content. Sulfate and chloride-rich samples also exhibited relatively low REE contents. In the basin, the REE contents of clay-rich samples were between 101.82 ppm and 162.04 ppm. In the carbonate-rich samples, the REE contents were between 36.82 ppm and 84.12 ppm. The REE contents of the sulfate-rich samples (anhydrite, gypsum and glauberite) ranged from 2.01 to 31.18 ppm, and in the purest anhydrite samples (T1-252.3 and T1-303) 2.01 ppm and 3.2 ppm, respectively (Tables 2 and 3).

In order to determine the origin of the sedimentary units in the basin, the REE contents of the samples were normalized to Chondrite [27],[28] and PAAS (Post-Archean Australian Shale) [29]. The carbonate containing clay-rich samples showed homogeneous the PAAS-normalized REE patterns, whereas evaporite samples exhibited variable REE patterns (Figure 7). The PAAS-normalized REE patterns of the sulfate-rich samples were similar to the chlorite-rich samples. According to PAAS, Eu anomaly varies between 1.0 -1.43 and a positive anomaly is observed. The lowest Eu anomaly (1.00) was found in the glauberite-rich sample. Ce anomaly varies between 0.80 -1.17. The Ce anomaly was either not observed or negative in the sediments except for carbonate and sulfate-rich two samples (T1-241:1.11 and T1-252.3:1.17) (Table 3).

4.2

0.08

15.40

0.20

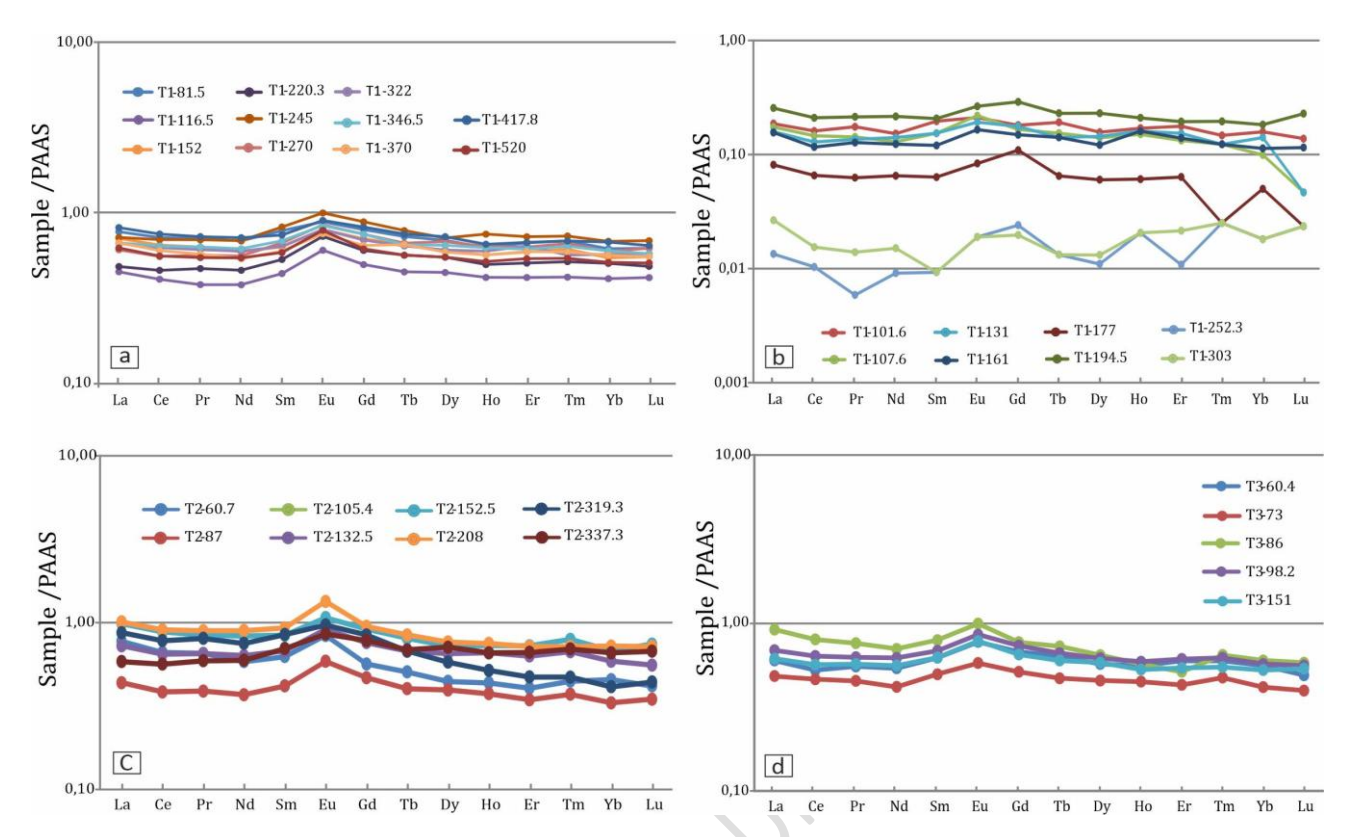


Figure 7 PAAS-normalized REE patterns of the Temelli basin samples. a) carbonate containing clay-rich samples of T1 drilling, b) evaporite-rich samples of T1 drilling, c) carbonate containing clay-rich samples of T2 drilling, d) carbonate containing clay-rich samples of T3 drilling.

	Table 2. Trace element contents (ppm) of the samples selected from drillings																
Sample	Ba	Ni	Sc	Be	Co	Cs	Ga	Hf	Nb	Rb	Sr	Ta	Th	V	W	Zr	Y
T1-81.5	230	100	14	2	17.3	11.2	32.3	3.7	15.1	116.8	141.6	1	11	100	1.3	140.1	18.1
T1-101.6	70	64	3	<1	4.9	2.1	2.7	8.0	3.3	19.6	528.8	0.3	2	39	1	31	4.3
T1-107.6	299	46	3	<1	5.1	1.6	2.3	0.8	2.3	19	7202.9	0.1	1.5	34	< 0.5	31.7	4.1
T1-116.5	564	116	8	3	15.8	3.5	7.4	2	7.6	45.3	10061.4	0.4	4.1	82	0.6	78	10.5
T1-131	116	61	4		6.2	2.4	2	0.7	2	22.1	1962.6	< 0.1	1.3	38	< 0.5	26.7	4.7
T1-152	219	80	11	2	14.8	11.4	15.6	2.9	13.5	102.2	127.4	0.9	9.5	79	1.7	123.7	15.2
T1-161	87	34	3	<1	4.7	3.4	1.5	8.0	3.3	20.4	1592.9	0.2	2	29	< 0.5	33.3	2.7
T1-177	65	<20	1	<1	1.7	0.9	< 0.5	0.6	1.3	9.7	1376.5	0.2	0.7	18	< 0.5	21.8	1.7
T1-194.5	79	57	4	<1	7.4	3.6	3.4	1.3	5.4	34.5	623.7	0.4	3.5	55	< 0.5	42.8	5.8
T1-220.3	193	147	12	3	21	10	10.5	2.4	10.5	70.6	415.4	0.6	5.3	92	1	96.9	13.6
T1-241	138	23	3	<1	4	2.2	2.9	1.5	4.5	28.8	1391	0.2	4	22	< 0.5	66	5.1
T1-245	319		22	4	27.2	14.2	18.4	3.6	14.9	131.8	263.6	0.9	10.7	143	2.3	135.6	18.1
T1-252.3	11	<20	<1	<1	< 0.2	0.1	< 0.5	0.1	0.4	8.0	1304.8	0.1	< 0.2	<8	< 0.5	3.8	0.5
T1-270	272	168	16	1	25.4	6.2	14.4	2.8	12.5	85.6	454.1	8.0	7.8	133	1.5	107.9	15.7
T1-303	8	<20	<1	<1	0.3	0.1	< 0.5	< 0.1	< 0.1	1.9	1321.1	< 0.1	< 0.2	<8	< 0.5	2.8	0.4
T1-322	365	116	11	5	22.4	6.7	11.5	3.1	12.1	77.2	544.2	8.0	9	100	1	120.8	14.8
T1-346.5	429	77	10	4	14.7	5.7	12.5	3.4	12.6	72.7	504.2	8.0	9	76	1.2	132.9	15.6
T1-370	365	67	9	1	12.9	9.5	11.4	3	12.9	94.2	560	8.0	9.3	79	1.5	123	15.3
T1-417.8	371	69	12	3	14.4	6	12.5	3	14.3	85.5	959.8	0.7	11	61	1.3	121.8	17.2
T1-520	317	66	10	<1	12.2	7.7	11.1	2.9	11.2	96.4	620.8	8.0	8.3	57	1	116.6	13.2
T2-60.7	205	109	13	1	12	20.8	14.9	3.6	14	119.8	230.7	1	9.4	80	1.5	133.6	10.4
T2-87	161	56	7	2	16.9	9.3	6.3	2.1	7.1	51.5	958.3	0.5	4.9	53	1.1	73.9	10.3
T2-105.4	377	77	10	1	12.8	5.5	11.4	4.8	17.2	76.3	720.8	1.2	10.7	73	1.4	194.1	19.8
T2-132.5	313	73	8	1	15.6	4.4	7.9	3.4	9.8	66.4	870.7	0.7	7.5	70	1.3	136.8	17.5
T2-152.5	936	97	12	1	17.7	5.7	12.6	4.3	16.7	82.5	624.3	1	10.2	73	1.5	184.2	19.9
T2-208	468	88	12	2	17.2	5.8	12.5	4.3	16.3	84.4	632.1	1	11	85	2.1	172	21.2
T2-319.3	239	135	8	2	36.7	9.6	16.1	5.2	16.5	141.9	127.6	1.3	14.1	74	2.5	187.9	14
T2-337.3	239	54	17	<1	12.2	26.1	15.3	3.4	11.8	139.6	156.4	8.0	7.4	130	12.9	131.8	17.9
T3-60.4	152	130	12	<1	17	5.2	11.1	3.3	13.9	69.8	541.5	0.9	8.5	103	1.7	124.7	15
T3-73	230	66	8	2	12	4.1	8.9	2.3	9.8	53.7	1165.1	0.4	7.2	196	1.1	86	11.7
T3-86	150	152	12	1	16.2	8.2	16.5	4.2	18.9	106	373.8	1.1	11.2	83	1.4	163.3	15.8
T3-98.2	115	107	12	1	16.4	5.9	10.7	3	11.5	69.9	1597.8	8.0	8.3	72	1.2	114.3	16.1
T3-151	117	104	10	2	16.5	5.3	9.1	3.5	11.3	55.3	505.3	0.7	7	78	1.2	134.1	14.7

In the chondrite-normalized REE patterns, LREE (light REE) were observed to be enriched relative to the HREE (heavy REE) (Figure 8). The Eu anomaly varies between 0.65 -0.93 and a negative in the basin sediments. The lowest Eu anomaly (0.65)

was found in the glauberite-rich sample. Ce* anomaly is similar to PAAS and varies between 0.83-1.22 (Table 3).

The LREE/HREE ratios of the drilling samples vary between 16.5 and 44.19. It was determined that LRE elements showed significant enrichment compared to HRE elements (Table 3).

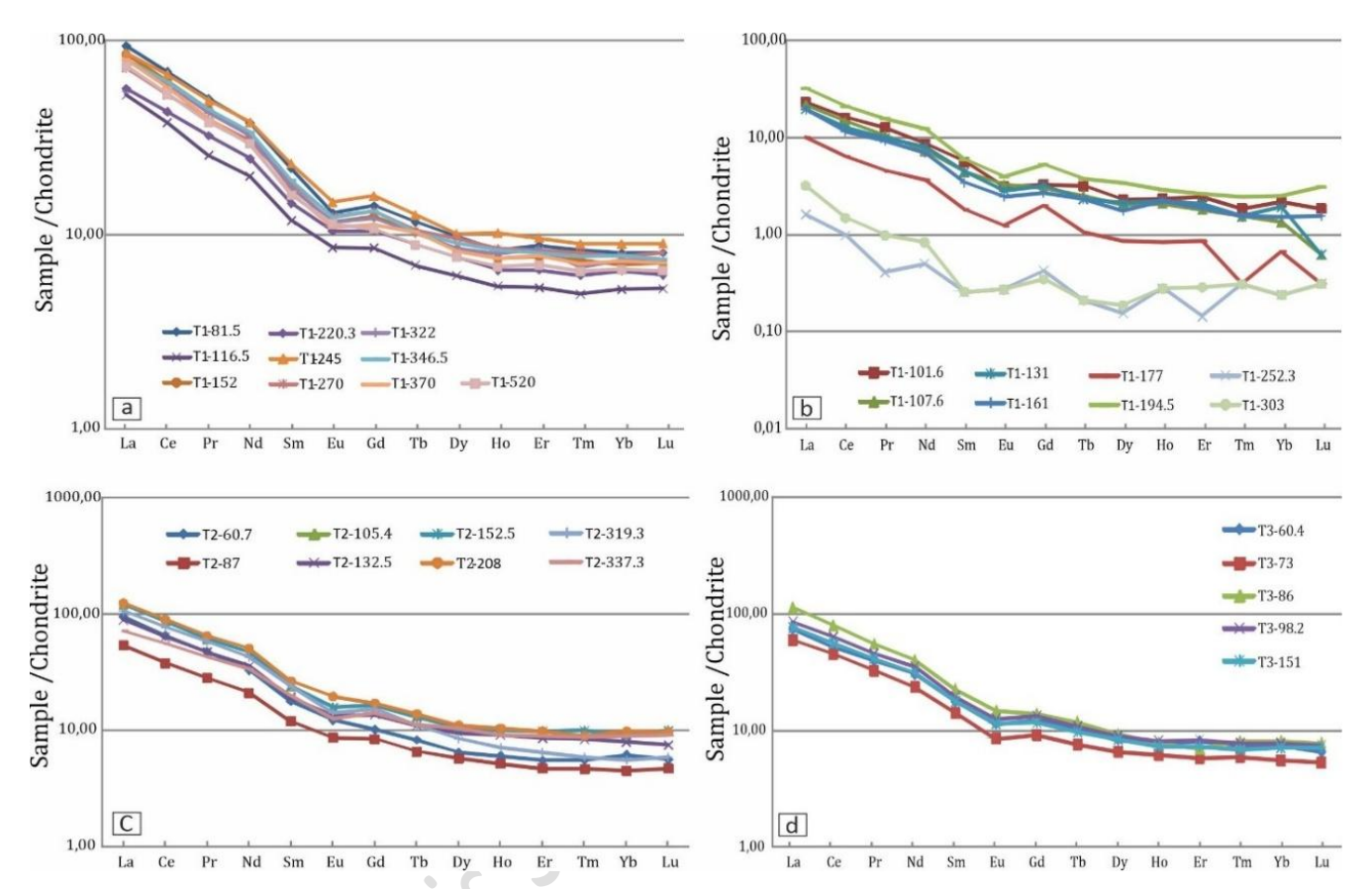


Figure 8 Chondrite-normalized REE patterns of the Temelli basin samples. a) carbonate containing clay-rich samples of T1 drilling, b) evaporite-rich samples of T1 drilling, c) carbonate containing clay-rich samples of T2 drilling, d) carbonate containing clay-rich samples of T3 drilling.

Table 3. Rare earth element (REE) contents (ppm), anomalies and ratios of the samples selected from drillings Chondrite PAAS Sample La Ce Pr Nd Sm Eu Gd Tb Dv Ho Er Tm Yb Lu REE Eu/Eu* Ce/Ce* Eu/Eu* Ce/Ce* HREE 0.26 T1-81.5 291 55.8 6.11 22.6 4.29 0.95 3.66 0.55 3 1 5 0.6 1.85 0.27 1.68 130.9 27.98 1.13 0.97 0.73 1.01 7.2 T1-101.6 12.9 1.56 5.2 1.1 0.23 0.85 0.15 0.74 0.17 0.51 0.06 0.45 0.06 31.2 24.87 1.12 0.89 0.73 0.93 0.90 T1-107.6 4.4 0.24 0.38 0.05 0.28 0.02 32.97 0.93 0.97 6.7 11.7 1.27 0.86 0.78 0.12 0.66 0.15 27.1 1.38 2.21 1.09 24.38 1.31 0.99 0.85 1.03 T1-116.5 16.3 30.5 3.13 12 2.31 0.63 0.33 1.98 0.39 1.12 0.16 0.17 72.3 0.83 0.87 0.76 T1-131 10.3 4.8 0.86 0.21 0.68 0.05 0.02 26.2 24.63 0.91 6.1 1.21 0.11 0.16 0.44 0.4 1.17 5.39 0.85 T1-152 50 3.21 0.49 2.7 0.54 0.24 1.47 0.23 115.8 28.40 1.21 0.97 0.79 1.01 26.4 19.3 3.4 1.62 T1-161 9.3 1.13 4.2 0.67 0.18 0.7 0.11 0.57 0.16 0.4 0.05 0.32 0.05 23.8 25.16 1.24 0.82 0.80 0.86 6 T1-177 5.2 0.55 2.2 0.35 0.09 0.51 0.05 0.28 0.06 0.18 0.01 0.14 < 0.01 12.7 32.50 1.00 0.92 0.65 0.96 T1-194.5 28.66 16.9 1.91 7.4 1.16 0.29 1.37 0.18 1.09 0.21 0.08 0.52 0.1 41.7 1.08 0.90 0.70 0.94 T1-220.3 34.7 3.95 14.8 2.83 0.77 2.71 1.38 0.2 83.9 22.63 1.00 17.6 0.42 2.47 0.47 0.2 1.36 1.31 0.96 0.85 T1-241 7.9 16.8 0.25 1.02 0.91 0.51 0.09 0.53 0.08 36.8 26.48 0.74 1.54 5.8 1.06 0.15 0.18 1.13 1.11 1.16 T1-245 26.8 54.1 5.99 22.7 1.08 3.26 0.73 2.02 0.29 1.87 0.29 128.4 24.52 1.18 0.99 0.77 1.03 4.53 4.1 T1-252.3 0.5 8.0 0.05 < 0.3 < 0.05 < 0.02 0.11 < 0.01 < 0.05 < 0.02 < 0.03 < 0.01 < 0.05 < 0.01 2.01 16.50 1.27 1.17 0.82 1.22 T1-270 22.4 42.4 4.8 18.2 3.6 0.91 3.43 0.5 3.09 0.61 1.74 0.26 1.62 0.26 103.8 22.63 1.22 0.94 0.79 0.98 < 0.05 < 0.02 0.09 < 0.01 0.91 T1-303 1.2 0.12 0.5 0.06 < 0.02 0.06 < 0.01 < 0.05 < 0.01 3.2 21.69 1.40 0.80 0.83 T1-322 24.6 48.2 5.19 19.5 3.42 0.85 3.15 0.48 2.74 0.57 1.77 0.22 1.55 0.24 112.5 25.79 1.22 0.98 0.79 1.03 T1-346.5 24.8 49.3 20.2 3.71 0.9 0.49 2.93 0.6 1.69 0.25 0.24 1.19 0.98 0.77 1.03 5.4 3.43 1.63 115.6 26.17 4.87 8.0 2.91 0.23 0.23 107.6 0.97 0.80 T1-370 17.5 3.19 0.49 0.54 1.63 25.79 1.01 24.8 46.2 2.66 1.53 1.24 0.97 0.27 0.97 0.76 T1-417.8 58.7 6.27 4.03 3.8 0.57 0.63 1.85 0.27 28.13 1.02 30.9 23.7 3.32 1.86 137.1 1.17 0.84 T1-520 42.7 4.63 17.7 3.13 2.47 0.49 1.47 0.21 1.38 0.21 101.4 26.92 0.95 0.87 1.00 0.42 1.34 19.7 0.18 0.91 T2-60.7 29.4 52.5 5.75 3.46 0.9 2.62 0.39 2.07 0.43 1.15 1.28 0.18 120.0 38.48 1.41 0.93 0.97 T2-87 30.5 3.42 12.5 2.31 0.63 2.17 0.31 1.84 0.37 0.98 0.15 0.93 0.15 72.9 28.52 1.33 0.93 0.86 0.97 16.6 T2-105.4 69.7 7.39 28.1 4.64 1.15 4.25 3.37 0.72 2.06 0.32 1.9 0.32 162.0 31.02 1.22 0.97 0.79 1.01 37.5 0.62 T2-132.5 27.6 51.2 21.4 3.75 0.98 3.52 0.52 3.04 0.65 1.65 0.24 122.3 26.82 1.27 0.94 0.82 0.98 0.79 T2-152.5 28.3 3.45 0.74 2.09 0.31 1.96 0.29 31.02 1.01

T2-208	38.4	71.6	7.86	30.2	5.13	1.44	4.4	0.65	3.56	0.74	2.04	0.29	2.03	0.31	168.7	31.70	1.43	0.95	0.93	0.99
T2-319.3	33.1	61.8	7.07	25.3	4.69	1.04	3.91	0.52	2.7	0.51	1.34	0.19	1.16	0.19	143.5	44.19	1.14	0.93	0.74	0.97
T2-337.3	22.2	44.7	5.19	20.1	3.87	0.92	3.62	0.53	3.32	0.65	1.88	0.28	1.85	0.29	109.4	21.44	1.16	0.96	0.75	1.00
T3-60.4	22.7	41.4	4.84	18.1	3.43	0.83	3.13	0.49	2.65	0.55	1.69	0.24	1.56	0.21	101.8	23.52	1.19	0.91	0.77	0.95
T3-73	18.3	36.5	3.96	14	2.73	0.62	2.37	0.36	2.11	0.44	1.21	0.19	1.16	0.17	84.12	26.65	1.15	0.99	0.75	1.03
T3-86	34.9	63.4	6.67	23.7	4.38	1.07	3.57	0.56	3	0.56	1.45	0.26	1.68	0.25	145.5	35.35	1.27	0.96	0.83	1.00
T3-98.2	26.2	50.4	5.49	20.9	3.78	0.92	3.4	0.51	2.87	0.58	1.73	0.25	1.6	0.24	118.9	26.96	1.21	0.97	0.78	1.01
T3-151	23.3	44.7	5	18.8	3.44	0.84	3.01	0.46	2.7	0.52	1.53	0.22	1.47	0.23	106.2	26.61	1.23	0.96	0.80	1.00

Note: $Eu/Eu^*=Eu_N/[Sm_NGd_N]^{1/2}$, $Ce/Ce^*=Ce_N/[La_NPr_N]^{1/2}$, REE (Rare Earth Element)=La-Lu, LREE (Light Rare Earth Element=La-Nd, HREE (Heavy Rare Earth Element)=Er-Lu

5 Discussion

5.1 The precipitation of evaporites

The evolution of the precipitated nonmarine evaporite minerals during the progressive evaporation were explained using chemical, mineralogical data and Eugster and Hardie's [30] pathways. The initial precipitation is depending on the Mg/Ca ratio of the parent brine. Firstly, precipitate minerals are calcite and aragonite in the evaporite basins. The following precipitation of a mineral sequence of sulfates, silicates and chlorides is controlled by the relative concentrations of calcium, magnesium, sulfate and bicarbonate ions in the brackish inflow waters. As calcite precipitates through evaporative concentration or other forcing mechanisms, the first precipitated calcite typically contains little or no Mg. As calcite precipitation progresses, the Mg/Ca ratio increases. In the absence of significant recharge, continued calcite precipitation results in elevated Mg/Ca ratios and the formation of Mg-bearing carbonates, such as dolomite, in highly concentrated lake environments [31],[32]. Calcite and dolomite are the main carbonate minerals in the Temelli Basin. Calcitegypsum/anhydrite-(dolomite) association and abundance of the calcite indicates a relatively dilute brine rich in Ca²⁺, Mg²⁺, CO₃- and SO₄-, and presence of a low salinity environment. The intermittent occurrence within the middle part of the sequence implies short-term salinity fluctuations, possibly related to episodic flooding. Further evaporation under the condition of high alkalinity and salinity led to the precipitation of sulfate and chloride minerals in major amounts.

The relative dominance of dolomite over calcite in the central and intermediate part of the basin, suggests high salinity conditions favored. Müller et al. [31] interpreted the dolomites in many salt lakes as predominantly secondary alteration products; however, more recent studies have reported the widespread occurrence of primary dolomite in other sedimentary basins. According to XRD analysis, the dolomites are rich in Ca²+ ion, and high-calcian dolomites (d₁₀₄ spacing ranges from 2.89 Å to 2.90 Å) [13]. This is non-stochiometric and less ordered than 'ideal' dolomite. Based on the results of mineralogical and geochemical analyses, the dolomites are defined as protodolomite, and these dolomite rhombs are interpreted to be authigenic under evaporitic conditions.

Gypsum/anhydrite-calcite-dolomite association and abundance of the gypsum and/or anhydrite in the sulfate-rich facies indicates a relatively high salinity environment. This association is widespread in the central and intermediate part of the basin. Anhydrite is widely regarded as a diagenetic mineral, representing the primary phase formed by the dehydration of microcrystalline gypsarenite [33],[34]. Nodular anhydrites occur within clayey and carbonate layers of the Temelli basin. Their presence is interpreted as an early diagenetic feature associated with exposure to terrestrial effect [35],[36]. During this dissolution and reprecipitation processes, the anhydrite nodules also formed.

Halite is the final evaporite product and the dominant evaporate mineral in the drillings. anhydrite/(gypsum)-analcime-dolomite-(calcite)-glauberite)] association in the chloride rich facies indicates a strong alkaline environment under relatively arid conditions resulting in halite, Na-bearing sulfate and analcime, elevated in concentrations of Na+ and Mg2+. The presence of the zeolite mineral analcime (Na(AlSi₂O₆)H₂O) is important, with occurrences reported in both ancient and modern saline lacustrine settings [37]-[39]. Analcime typically forms under conditions of relatively high salinity and alkalinity, in a more central part of the saline alkaline lake basin compared to other zeolite minerals (e.g. [40]). In such environment, the formation of analcime is promoted by high Na⁺/H⁺ ratios, low Si/Al ratios, and low H₂O activities [41]. The sediments of Temelli basin intercalated to volcanic and pyroclastic rocks. Analcime occurs as a result of diagenetic interaction between saline solutions and precursor volcanic glass in pyroclastic sediments.

Hardie [42] interpreted glauberite is an authigenic mineral and it typically formed by the reaction of previously deposited gypsum with Na-rich brines. The reaction [43] is as follows:

$$2CaSO_4.2H_2O_{(s)} + 2Na_{(aq)} \rightarrow CaSO_4.Na_2SO_{4(s)} + Ca_{(aq)} + 4H_2O$$

Glauberite formation has also been attributed to complex diagenetic processes, wherein various mineral assemblages—comprising mirabilite, bloedite, thenardite, and halite—are systematically replaced by glauberite under the influence of Carich groundwater solutions [44]. In such settings, glauberite represents a syngenetic interstitial precipitate that forms during the final stages of evaporitic evolution in playa environments and is typically found at the base of halite layers, as observed in the basin. It is observed that glauberite formed from halite in SEM observations. Lenticular and bar shaped glauberite crystals were found together with halite in SEM and mineralogical analysis. Dissolution traces were detected on the surface of halite (Figure 5j).

5.2 Geochemical implications

Temelli basin carbonate and sulfate samples presented large differences in their strontium levels. Sr contents of carbonate and sulfate minerals reflect depositional conditions of the environment. Salinity has been assumed to be the primary factor controlling strontium coprecipitation in gypsum, therefore, the strontium content is often used as an indicator of salinity within gypsum-bearing facies [45]. Very low Sr contents in the samples also indicate that this gypsum grew under pressure at low salinity. However, anhydrite and glauberite sample have higher Sr contents than the gypsum samples, and these high Sr contents indicate that the sulfate minerals formed in higher salinity than did the gypsum. Calcite rich samples have lower Sr contents than dolomite rich samples. The low Sr values of calcite samples may reflect a decline in salinity conditions, possibly associated with basin deepening or freshwater input, while elevated Sr values of dolomite rich samples could reflect increasing salinity conditions. Homogeneous strontium contents reflect deposition under conditions of hydrological stability and relatively deep waters, but more variable strontium content relates, in accordance with other sedimentological criteria, to a shallowing of the basin [45],[46]. Therefore, the large differences in strontium content (528.8–10,061.4 ppm) observed in the carbonate and sulfate units of the Temelli basin evaporites may reflect deposition under fluctuating hydrological conditions and in shallow water environments.

Sholkovitz and Szymezak [47] observed that under low salinity conditions, dissolved light rare earth elements (LREEs) are preferentially removed from solution, whereas high salinity conditions tend to favor the removal of heavy rare earth elements (HREEs). Additionally, pH plays a critical role: under acidic conditions, REEs tend to remain in solution, while under alkaline conditions, they are more likely to precipitate or be adsorbed onto clay and hydroxide minerals [48]. In low pH (<3) aquatic environments, LREEs tend to remain as dissolved species, whereas HREEs-and to a lesser extent, MREEs (Middle Rare Earth Elements)—are preferentially adsorbed onto particle surfaces. This behavior is generally attributed to the stronger affinity of Fe-oxyhydroxides for HREEs, leading to their preferential scavenging from solution [49]. In contrast, in non-acidic water environments (pH > 6), light rare earth elements (LREE) tend to be preferentially adsorbed onto particles, whereas heavy rare earth elements (HREE) tend to stay in the solution [50]. However, one cannot except the possibility that this is due to changes in clay mineralogy and other mineral phases or the organic matter content. HREE concentrations in aquatic systems are generally associated with high levels of dissolved organic carbon and/or a low pH [51],[52]. Thus, the relatively high alkaline conditions of the basin may explain the low HREE levels in the evaporite samples.

REEs may be released into the water during dolomitization, as calcite contains significantly higher concentrations of REEs compared to dolomite within the basin. The sulfate and chloride-rich samples exhibit a variable REE pattern, whereas clay rich samples and carbonate samples show a homogeneous REE pattern in the basin (Fig. 7 and 8); The observed fractionation of rare earth elements could potentially be explained by their complexation with Cl⁻ [53]. Supporting evidence for this includes not only the high Cl⁻ concentrations in the brines, but also the stability constant plots of REE-Clcomplexes, which display an inverse mirror image of the REE distribution patterns observed in the most fractionated samples. In the initial stage, this process may lead to a depletion of LREEs in the solid phase, as LREEs preferentially remain in the fluid. However, with progressive precipitation, the residual fluid becomes enriched in LREEs, which may eventually offset their increased solubility and facilitate their incorporation into subsequent mineral phases [54].

Similar REE distribution indicates that REE is originated from the same origin. Eu anomalies are typically interpreted as being inherited from the source rocks, while Ce anomalies often result from post-deposition [55],[56]. When the REE contents of various sedimentary rock types in the upper continental crust were normalized to chondrite, enrichment in light REEs, a negative Eu anomaly and relatively flat heavy REE patterns were observed [57]. Thus, according to chondrite, negative Eu anomaly and LRE element enrichment relative to HRE elements in the sediments indicated that the basin is upper continental crust origin. According to PAAS, the positive Eu anomaly confirms a volcanic origin. There are various rocks around the

basin, such as quartzite, calc-schist, coarse crystalline white marbles, basaltic pillow lava, volcanoclastic conglomerate-sandstone alternations, volcanic and pyroclastic rocks. The Eu anomalies detected in the basin are interpreted to originate from these lithological sources.

6 Conclusions

Temelli Neogene basin is a tectonic controlled, large, closed lake and contains syngenetically deposited sediments. The basin is associated with other Neogene basins in the area. Local field study was done and samples were collected from various locations within the study area and also deep drillings. A substantial buried sedimentary sequence, approximately 500 meters thick and composed of fluvial and lacustrine deposits, has been identified in the Temelli Neogene basin. The mineralogical composition of the basin includes dolomite, calcite, anhydrite, glauberite, halite, and gypsum, along with feldspar, quartz, Ca-smectite, Na-smectite, illite, chlorite, kaolinite, and analcime. The vertical and lateral facies development of evaporitic and non-evaporitic units was identified. Evaporitic units, indicative of arid climatic periods, are thicken in the central parts of the basin to the northwest, whereas non-evaporitic units are mainly located in the eastern and southern margins in the basin.

In general, carbonate-rich sediments (mainly calcite and dolomite) reflect low-salinity conditions and a relatively high lake level, while sulfate-rich sediments (mainly gypsum, anhydrite, and glauberite) indicate elevated salinity associated with a lower lake stand. In addition, chloride-rich (mainly halite) sediments point very high salinity environments and a relatively low lake level. Evaporite and evaporite/carbonate minerals were precipitated during the arid and semiarid conditions that prevailed in this basin. By revealing the distribution and characteristics of the economically important mineralizations determined within the basin, future studies will be directed to the large Polath basin, which includes many sub-basins.

 Ca^{2+} and Na^+ are the dominant major cations in both carbonate and evaporitic rocks. Al_2O_3 and SiO_2 contents are notably higher in the clayey layers. Rare earth elements (REEs), along with some other trace element (V, Sc, Cr, Co, As, Ba, Rb, and Th) contents, are higher in clay-rich samples compared to evaporite-rich ones. The wide range of Sr concentrations (528.8–10,061.4 ppm) observed in the carbonate and sulfate units suggests deposition under hydrologically unstable and shallow water conditions. LRE element enrichment relative to HRE elements and Eu anomaly indicated that the basin is upper continental crust origin and fed from a volcanic source.

7 Acknowledgement

8 Author contribution statements

Author took part in literature research, construction, and writing of the experiments, the study's experimental study process and provided control.

9 Ethics committee approval and conflict of interest statement

There is no need to obtain permission from the ethics committee for the article prepared.

There is no conflict of interest with any person / institution in the article prepared.

10 References

- [1] Ünalan G, Yüksel V, "Eski Bir Graben Örneği: Haymana-Polatlı Hayzası". *Türkiye Jeoloji Bülteni*, 21, 165-169, 1978.
- [2] Görür N, Tüysüz O, Şengör AMC. "Tectonic Evolution of the Central Anatolian basins". *International Geology Review*, 40:831–850. 1998.
- [3] Ercan T. "Orta Anadoludaki Senozoyik Volkanizması", Bulletin of the Mineral Research and Exploration, 107, 120-140, 1986.
- [4] Kocadere B. Malıköy (Polatlı-Ankara) Sıcak ve Mineralli Sularının Hidrojeokimyasal İncelenmesi, Yüksek Lisans Tezi, Hacettepe Üniversitesi, Ankara, Türkiye, 109. 2009.
- [5] Demirtaş R, Adil F. "Ankara İli, Polatlı İlçesi, Temelli Beldesi, İ28-b1 ve İ28-b4 Paftaları İçinde Kalan Alanın Arazi Kullanımına Esas Jeolojik Etüt Raporu." Ankara, Türkiye, 52, 2010.
- [6] Temel A, Yürür T, Alıcı P, Varol E, Gourgaud A, Bellon H, Demirbağ H. "Alkaline series related to Early-Middle Miocene intra-continental rifting in a collision zone: An example from Polatlı, Central Anatolia, Turkey", Journal of Asian Earth Sciences 38 (2010), 289–306, 2010.
- [7] Esat K. Ankara Çevresinde Orta Anadolu'nun Neotektoniği ve Depremselliği, Doktora Tezi, Ankara Üniversitesi, Ankara, Türkiye, 160, 2011.
- [8] Küçükuysal C. Paleoclimatological Approach to Plio-Quaternary Paleosol-Calcrete Sequences in Bala and Gölbaşı (Ankara) by Using Mineralogical and Geochemical Proxies, Doktora Tezi, Middle East Technical University, Ankara, Türkiye, 271. 2011.
- [9] Hoşgör İ. Haymana-Polatlı Havzası Paleosen Mollusklarının Taksonomik Tanımlanması, Paleoekolojisi, Paeocoğrafyası ve Bentik Foraminiferlerle Biyostrartigrafik Deneştirilmesi, Doktora Tezi, Ankara Üniversitesi, Ankara, Türkiye, 145, 2012.
- [10] Bilgin AZ, Uğuz MF, Sevin M, Parlak O, Pekgöz M, Elibol H, Erdem Y, Özden U A. "Ayaş-Temelli-Polatlı (Ankara) Dolayının Jeolojisi." MTA Genel Müdürlüğü, Ankara, Türkiye, 11215, 2009.
- [11] Bilgin A Z. "Türkiye Jeoloji Haritaları Ankara İ-28 Paftası." MTA Dergisi, Ankara, Türkiye, 208, 2014.
- [12] Kaya İS. Temelli-Yenikent-Anadolu Otoyolu Bağlantı Yolunun Jeolojik ve Jeoteknik Değerlendirilmesi, Doktora Tezi, Süleyman Demirel Üniversitesi, Isparta, Türkiye, 255, 2015.
- [13] Altay T, Yağmurlu F, Şentürk M, Murat A. "Temelli (Ankara) Neojen Havzasındaki Sedimanter Birimlerin Jeolojisi ve Mineralojisi ile İlgili İlk Verilerin Değerlendirilmesi." Afyon Kocatepe Üniversitesi Fen Bilimleri Dergisi, 17(3), 1096-1108, 2017.
- [14] Akıllı H, Mutlu H. "Polatlı ve Haymana (Ankara) sıcak sularının kökenine yönelik kimyasal ve izotopik sınırlamalar." *Yerbilimleri*, 39(1), 41-64, 2018.
- [15] Gülyüz E, Özkaptan M, Kaymakci N, Persano C, Stuart FM. "Kinematic and thermal evolution of the Haymana Basin, a fore-arc to foreland basin in Central Anatolia (Turkey)." *Tectonophysics*, 766, 326-339, 2019.
- [16] Hoşgör İ, Pacaud JM. "New pareorine gastropod species from the Danian (Paleocene) of the Haymana-Polatlı Basin, Central Turkey." *Bollettino della Società Paleontologica Italiana*, 61(3), 279-287, 2022.
- [17] Güney R, Özerk ZR, Izladı E, Erden S, Aka E, Apatay E, Eryılmaz E, Yıkmaz B, Özdemir SA, Gündüz S, Can T, Çelik

- İ, Gürer A, Aykaç S, Arısoy MÖ, Köse EB, Demirci BB. "Evaporate salt exploration by two-dimensional (2D) seismic reflection method: Ankara-Polatlı region, Central Turkey." *Bulletin of the Mineral Research and Exploration*, 170(170), 1-17, 2022.
- [18] Özer S, Sasaran L. "Taxonomic revision of the canaliculate radiolitid (rudist, bivalve) genus *Lattenbergites* Lupu, 1987 from the Upper Cretaceous of the central and eastern Mediterranean Tethys: palaeobiogeographic distribution." *Cretaceous Research*, 152, 105684, 2023.
- [19] Erol O. "Ankara güneydoğusundaki Elma Dağı ve çevresinin jeolojisi ve jeomorfolojisi üzerinde bir araştırma." *Maden Tetkik ve Arama Enstitüsü Yayını*, Seri D. No:9, 1956.
- [20] Çalgın R, Pehlivan H, Ercan T, Şengün M. "Ankara Civarının Jeolojisi." Maden Tetkik ve Arama Enstitüsü, Ankara, Türkiye, 6487, 1973 (Yayınlanmamış).
- [21] Akyürek B, Bilginer E, Akbaş B, Hepşen N, Pehlivan Ş, Sunu O, Soysal Y, Dağer Z, Çatal E, Sözeri B, Yıldırım H, Hakyemez Y. "Ankara-Elmadağ-Kalecik dolayının jeolojisi." Maden Tetkik ve Arama Enstitüsü, Ankara, Türkiye, Rapor No: 7298 (yayımlanmamış), 1982.
- [22] Akyürek B, Bilginer E, Akbaş B, Hepşen N, Pehlivan Ş, Sunu O, Soysal Y, Dağer Z, Çatal E, Sözeri B, Yıldırım H, Hakyemez Y. "Ankara-Elmadağ-Kalecik dolayının temel jeolojik özellikleri." Türkiye Jeoloji Kurumu Bülteni, 20, 31-46, 1984.
- [23] Türkecan A, Dinçel A, Hepşen N, Papak i, Akbaş B, Sevin M, Özgür İB, Bedi Y, Mutlu G, Sevin D, Ünay E, Saraç G, Karataş S. "Bolu-Çankırı (Köroğlu Dağları) arasındaki Neojen yaşlı volkanitlerin stratigrafisi ve petrolojisi", Türkiye Jeoloji Bülteni 6, 85-103, 1991.
- [24] Uğuz MF, Turhan N, Bilgin AZ, Umut M, Şen AM, Acarlar M. "Kulu (Konya), Haymana (Ankara) ve Kırıkkale dolayının jeolojisi", MTA Genel Müdürlüğü Rapor No: 10399, Ankara, 1999.
- [25] JCPDS. Mineral Powder Diffraction File Databook. Joint Committee on Powder Diffraction Standards, Swarthmore, Pennsylvania, 781p, 1993.
- [26] Semiz B. "Pamukkale (Denizli) Bölgesi Killerinin Karakteristik Özellikleri ve Seramik Sektöründe Kullanılabilirlikleri" Pamukkale Üniveristesi Mühendislik Bilimleri Dergisi, 24(6), 1237-1244, 2018.
- [27] Condie KC. "Chemical Composition and Evolution of the Upper Continental Crust; Contrasting Results from Surface Samples and Shales." *Chemical Geology*, 104, 1-37, 1993.
- [28] Boynton W V. "Geochemistry of rare earth elements: meteorite studies". Pp. 63–114 in: Rare Earth Element Geochemistry (P. Henderson, ed.). Elsevier, Amsterdam. 1984.
- [29] McLennan SM. "Rare earth elements in sedimentary rocks: influence of provenance and sedimentary processes". *Review of Mineralogy*, 21, 169-200, 1989.
- [30] Eugster HP, Hardie LA. Saline Lakes. In: Lerman A, ed. Lakes: Chemistry, Geology, Physics. New York, NY, Springer-Verlag, 237-293, 1978.
- [31] Müller G, Iron G, Förstner U. "Formation and diagenesis of inorganic Ca-Mg carbonates in the lacustrine environment." Naturwissenschaften, 59, 158-164, 1972.
- [32] Last WM. "Lacustrine dolomite an overview of modern, Holocene and Pleistocene occurrences." Earth-Science Reviews, 27, 221-263, 1990.
- [33] Murray RC. "Origin and diagenesis of gypsum and anhydrite." *Journal of Sedimentary Research*, 34(3), 512–523, 1964.

- [34] Holliday DW. "The petrology of secondary gypsum rocks: a review." *Journal of Sedimentary Petrology*, 40, 734-744, 1970.
- [35] Shearman DJ. "Origin of evaporites by diagenesis." *Trans. Inst. Min. Metall.*, 75, B208-215, 1966.
- [36] Holliday DW. "Secondary gypsum in middle Carboniferous rocks of Spitsbergen." Geological Magazine, 104(2), 171– 176, 1967.
- [37] Hay RL. "Zeolites and zeolitic reactions in sedimentary rocks." *Geological Society of America*, 130 (*Special Paper 85*), 1966.
- [38] Surdam RC, Eugster HP. "Mineral reactions in the sedimentary deposits of the Lake Magadi region, Kenya." *Geological Society of America Bulletin*, 87, 1739–1752, 1976.
- [39] Roy PD, Caballero M, Lozano R, Ortega B, Lozano S, Pi T, Israde I, Morton O. "Geochemical record of late Quaternary paleoclimate from lacustrine sediments of paleo-lake San Felipe, western Sonora desert, Mexico." *Journal of South American Earth Sciences*, 29, 586-596, 2010.
- [40] Gude AJ, Sheppard RA. "A zeolitic tuff in a lacustrine facies of the Gila Conglomerate near Buckhorn, Grant County, New Mexico." *United States Geological Survey Bulletin*, 1763, 22p, 1988.
- [41] Mees F, Stoops G, Van Ranst E, Paepe R, Van Overloop E. "The nature of zeolite occurrences in deposits of the Olduvai Basin, Northern Tanzania." *Clays and Clay Minerals*, 53(6), 659-673, 2005.
- [42] Hardie LA. "The origin of the recent non-marine evaporite deposit of Saline Valley, Inyo Country, California." Geochimica et Cosmochimica Acta, 32, 1279–1301, 1968.
- [43] Ortí F, Gündogan I, Helvaci C. "Sodium sulphate deposits of Neogene age: The Kirmir Formation, Beypazari Basin, Turkey." *Sedimentary Geology*, 146, 305–333, 2002.
- [44] Grokhovskii LM. "Glauberite as the source of sodium sulfate". *Lithology and Mineral Resources* (New York). 12/3, 356–360, 1978.
- [45] Rosell I, Ortí F, Kasprzyk A, Playà E, Peryt TM. "Strontium geochemistry of Miocene primary gypsum: Messinian of southeastern Spain and Sicily and Badenian of Poland." *Journal of Sedimentary Research*, 68, 63-79, 1998.
- [46] Matano F, Barbieri M, Di Nocera S, Torre M. "Stratigraphy and strontium geochemistry of Messinian evaporite-

- bearing successions of the southern Apennines foredeep, Italy: Implications for the Mediterranean 'salinity crisis' and regional palaeogeography." *Palaeogeogr. Palaeoclimatol. Palaeoecol.*, 217, 87–114, 2005.
- [47] Sholkovitz E, Szymezak R. "The estuarine chemistry of rare earth elements: comparison of the Amazon, Fly, Sepik and Gulf of Papua systems." *Earth and Planetary Science Letters*, 178, 299–309, 2000.
- [48] Johannesson KH, Zhou X. "Origin of middle rare earth elements enrichments in acid waters of a Canadian High Arctic Lake." *Geochimica et Cosmochimica Acta*, 61, 153-165, 1999.
- [49] Aström M. "Abundance and fractionation patterns of Rare Earth Elements in streams affected by acid sulphate soils." *Chemical Geology*, 175, 249-258, 2001.
- [50] Sholkovitz ER. "Chemical evolution of rare earth elements: fractionation between colloidal and solution phases of filtered river water." *Earth and Planetary Science Letters*, 114, 77–84, 1992.
- [51] Dupré B, Gaillardet J, Rousseau D, Allègre CJ. "Major and trace elements of river-borne material: The Congo basin." *Geochimica et Cosmochimica Acta*, 60, 1301-1321, 1996.
- [52] Gaillardet J, Dupre' B, Alle'gre JC, Ne'grel P. "Chemical and physical denudation in the Amazon River Basin." *Chemical Geology*, 142, 141–173, 1997.
- [53] Steinmann M, Stille P. "Strongly fractionated REE patterns in salts and their implications for REE migration in chloride-rich brines at elevated temperatures and pressures." C.R. Acad. Sci. Paris, Série II A, 327, 173-180, 1998.
- [54] Steinmann M, Stille P, Mengel K, Kiefel B. "Trace element and isotopic evidence for REE migration and fractionation in salts next to a basalt dyke." *Applied Geochemistry*, 16, 351-361, 2001.
- [55] McLennan SM. "Rare earth elements in sedimentary rocks: influence of provenance and sedimentary processes." *Reviews in Mineralogy*, 21, 170-199, 1989.
- [56] Pourret O, Davranche M, Gruau G, Dia A. "New insights into cerium anomalies in organic-rich alkaline waters." *Chemical Geology*, 251, 120-127, 2008.
- [57] Rudnick RL, Gao S. "Composition of the Continental Crust". Treatise on Geochemistry, 3:1-64, 2003.